Advances in Aircraft and Spacecraft Science, *Vol. 2, No. 2 (2015) 109-124*
DOI: http://dx.doi.org/10.12989/aas.2015.2.2.109

Assessment of the aerodynamic and aerothermodynamic performance of a high-lift reentry vehicle

Giuseppe Pezzella*

Fluid Dynamics Laboratory, Aerothermodynamics Section, Italian Aerospace Research Centre, via Maiorise I-81043 Capua, Italy

(Received July 18, 2013, Revised February 11, 2014, Accepted September 2, 2014)

Abstract. This paper deals with the aerodynamic and aerothermodynamic trade-off analysis of a hypersonic flying test bed. Such vehicle will have to be launched with an expendable launcher and shall re-enter the Earth atmosphere allowing to perform several experiments on critical re-entry phenomena. The demonstrator under study is a re-entry space glider characterized by a relatively simple vehicle architecture able to validate hypersonic aerothermodynamic design database and passenger experiments, including thermal shield and hot structures. A summary review of the aerodynamic characteristics of two flying test bed concepts, compliant with a phase-A design level, has been provided hereinafter. Several design results, based both on engineering approach and computational fluid dynamics, are reported and discussed in the paper.

Keywords: hypersonic flow; re-entry vehicles; aerodynamics; aerothermodynamics; computational fluid dynamics

1. Introduction

This paper deals with the aerodynamic and aerothermodynamic analysis of a reentry flight demonstrator helpful to research activities for the design and development of a possible winged Reusable Launch Vehicle (Russo 2001). Such experimental vehicle will have to be launched with an expendable launcher and shall re-enter the Earth atmosphere by means of a sub-orbital flight that shall be conducted at hypersonic Mach number, in the range 6-8 at moderate angles of attack (AoA) (Guidotti *et al*. 2011). During the flight a number of experiments on critical re-entry technologies shall be performed (Russo 2001). In particular, this design step allows researchers to gain confidence that a full-scale development can successfully proceed. In the paper some preliminary results of vehicle design are provided (Pezzella *et al*. 2011).

The flying test bed (FTB) configuration, namely FTB_4, is designed to be allocated in the fairing of a small launcher and to withstand to aero-thermal loads of the re-entry flight within a set of trajectories provided by the Flight Mechanics simulations. In order to get a trade-off study several configurations have been taken into account and the preliminary aerodynamic and heating databases have been produced, as input for both the Flight Mechanics and Thermo-Mechanics

*Corresponding author, Ph.D. Researcher, E-mail: g.pezzella@cira.it

http://www.techno-press.org/?journal=aas&subpage=7 ISSN: 2287-528X (Print), 2287-5271 (Online)

design analysis. Such aerodynamic data have been used to generate a number of possible re-entry trajectories, able to fulfil Programme requirements.

The present paper reports on several analysis tools integrated in the conceptual design process of a small hypersonic FTB especially for what concerns the vehicle's aerothermal design. Among others, we used computational analyses to simulate aerothermodynamic flowfield around the vehicle concept and surface heat flux distributions to design the vehicle thermal protection system (TPS). The vehicle detailed design, however, is beyond the scope of this work and the mission and system requirements will be defined only at the concept feasibility level.

The demonstrator under study is a re-entry space glider characterized by relatively simple vehicle architecture able to validate hypersonic aerothermodynamic design database and passenger experiments, including thermal shield and hot structures, giving confidence that a full-scale development can successfully proceed. A summary review of the aerodynamic characteristics of the FTB concepts, compliant with a phase-A design level, has been provided as well, according to the Space-Based design approach (Prabhu 2004).

Accurate aerodynamic analyses, however, are very complex and time consuming, and are not compatible with a phase-A design study in which fast predicting methods are mandatory. Therefore, the evaluation of the vehicle aerodynamic database (AEDB) was mainly performed by means of engineering tools, while a limited number of more reliable Computational Fluid Dynamics (CFD) computations were performed in order to verify the attained accuracy and to focus on some critical design aspects not predictable with simplified tools. The engineering-based aerodynamic analysis was addressed by using a 3-D Supersonic-Hypersonic Panel Method code (S-HPM) that computes the aerodynamic characteristics, including control surface deflections and pitch dynamic derivatives, of complex arbitrary three-dimensional shapes by using simplified engineering methods as Prandtl-Meyer expansion flow theory and tangent cone/wedge methods, together with the modified Newtonian one (Pezzella *et al*. 2009).

The code H3NS, developed at CIRA, was used to carry out the CFD analysis (Roncioni *et al*. 2009). It solves the thermal and chemical non equilibrium governing equations in a density-based approach with an upwind Flux Difference Splitting (FDS) numerical scheme for the convective terms. H3NS solves the full Reynolds Averaged Navier-Stokes equations in a finite volume approach, with a cell centered formulation on a multi-zone block-structured grid (Pezzella *et al*. 2009, Viviani and Pezzella 2010). For the numerical CFD simulations (continuum flow regime only) was chosen the non-viscous Euler approximation which, although not accounting for viscosity effects, it is sufficient for the prediction of surface pressure distribution, position and intensity of shock-shock wave interactions. Additional information about CFD analysis considered in the present research effort can be found in (Pezzella 2011).

2. Vehicle configuration

The vehicle shall be a concept embodying all the features of an operational system (De Matteis and Russo 2006). In particular it shall be characterized by a rather high aerodynamic efficiency, and therefore shall exhibit rather sharp nose and wing leading edges and shall fly at moderate AoA.

It will provide aerodynamic and aerothermodynamic flight data for correlation with ground test (e.g., Scirocco Plasma Wind Tunnel, PWT) results, thus providing new insight into the understanding of complex aerothermodynamic phenomena occurring in flight and improving

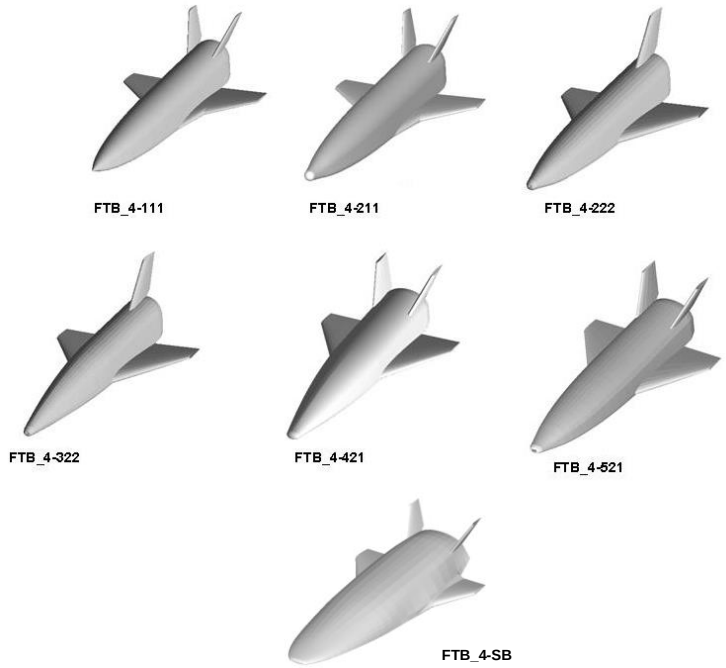

Fig. 1 FTB trade-off configurations

prediction methodologies and extrapolation to flight theory.

Among system requirements that directly impact on the aerothermal environment definition of vehicle, there is the use of a small expendable launch vehicle (ELV). This requirement is expected to have a strong impact on vehicle design as launcher fairings limit the overall dimensions of the vehicle. Anyway, the vehicle configuration shall be the result of trade-off design activities involving several design criteria as winged-body and lifting body configuration. For example, Fig. 1 shows several vehicle configurations involved so far in the trade-off design. As shown, within the family of lifting body the trade-off design relies also on spatuled-body (SB) configurations, namely FTB_4-SB, being characterized by interesting performances from the aerodynamic and aerothermodynamic point of view (Guidotti *et al*. 2011, Pezzella *et al*. 2011).

Of course, the winning configuration is the one showing, at the same time, the best aerodynamic and aerothermodynamic performance.

The typical aerodynamic configuration must feature a compact body with rounded edge delta-like fuselage cross section and delta planform wing as basic shape. The vehicle architecture must show a fuselage and a wing with a blended wing body interface and a flat bottomed surface to increase the concept hypersonic aerothermodynamic performance (i.e., the lower surface of the body provides a significant amount of lift at hypersonic velocities).

The wing size and location shall be defined on the basis of trade-off studies so to improve vehicle aerodynamics and provide static stability and controllability during flight. Further, the nose camber shall be determined in order to keep the aerodynamic center of pressure (CoP) close to the center of gravity (CoG). For instance, the cambered up nose increases the pitching moment coefficient (e.g., $Cm_0>0$), thus allowing to pitch-trim the vehicle with positive (i.e., downward) deflections of aerodynamic control surfaces.

The wing shall be swept back to assure best performance with respect to supersonic drag and aerodynamic heating. Up to now two wing concepts have been considered, namely wing #1 and #2. The wing sweep angle is equal to 45 deg for the wing #1 and 56 deg for the one #2.

Note that, as preliminary reference configuration, the wing #2 was not characterized by a strake because no requirements on landing exist. A properly designed strake could be added in the future, depending on the confirmation of a specific landing requirement. The trailing edge (TE) has a sweep forward angle of 6 deg.

A wing dihedral angle shall be also provided to enhance vehicle lateral-directional stability. The wing section shape shall feature a nearly flat bottomed surface to dissipate efficiently the aeroheating, while the leading edge shall be rather sharp in order to reduce wave drag. Moreover, the wing shall feature a high length-to-width ratio to minimize drag.

Control power for vehicle concept shall be provided by two wing flaps and ruddervators (recall that wing flaps used symmetrically – e.g., elevons – are the primary controls for the pitch axis; whereas roll control can be obtained through asymmetrical usage – e.g., ailerons).

The rudder helps to provide the directional control, i.e., sideslip stability. During entry, the rudder shall be augmented by reaction control system (RCS).

Note that the requirement to fly at moderate AoA along the re-entry implies that the tail is expected to be slightly more effective unlike a classical re-entry, (e.g., US Orbiter like), where at high AoA the Shuttle vertical fin is shielded from the flow, thus providing no control.

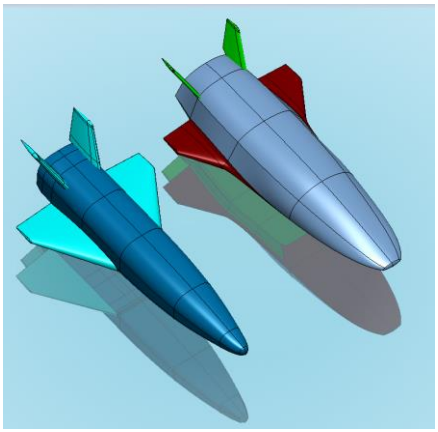

Fig. 2 Winged (FTB-4_421 or 521) and spatuled (FTB-4_SB) body configurations comparison

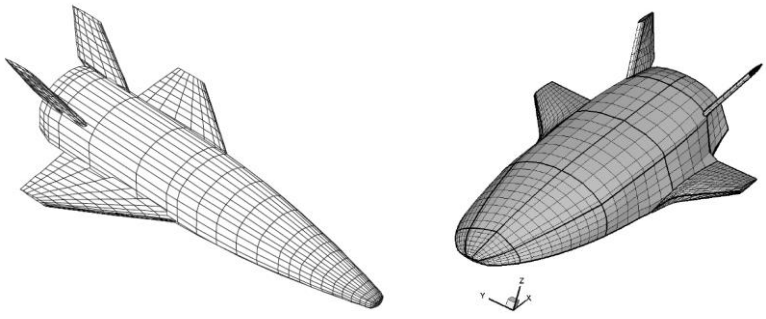

Fig. 3 Example of panel meshes

Finally, the vehicle may be provided by a body flap located at the trailing edge of the fuselage in order to augment pitch control and stability (trim capability to relieve elevon loads is obtained by body flap deflection).

The design results, hereinafter provided, refer, in particular, to FTB-4_421 and FTB-4_521 (both winged body, WB) and FTB-4_SB configurations, which are shown in Fig. 2. Note that, FTB-4_421 and 521 are quite similar. They differ only for the nose camber. The former is nose down cambered while the latter is nose up cambered.

3. Aerodynamic analysis

Concepts aerodynamics has been extensively addressed by means of Surface Impact Methods (SIM) typical of hypersonics, such as Prandtl-Meyer expansion flow theory and tangent cone/wedge method together with the Newtonian theory (Anderson 1989). Fig. 3 shows typical FTB_4 surface panel meshes that have been used for the engineering level computations (Brauckmann 1999, Maughmer *et al*. 1993).

In the following Fig. 4 to Fig. 8 some of the main results obtained for clean configuration aerodynamics (i.e., no control surface deflected) are shown. For example, Fig. 4 and Fig. 5 show the aerodynamic polars of all the competing configurations at M_∞=6.

As shown, the SB configuration is the best lifted one for all the AoA considered; while up to about α=5 deg the configuration FTB_4-521 shows the higher aerodynamic drag. This is due to combined effects of the higher planform and frontal area which characterize the spatuled body configuration (Moore and Williams 1989).

The pitching moment coefficients versus AoA at M_∞=7 for each FTB_4 configuration are recognized in Fig. 6 and Fig. 7. The pole for the calculation of the moment coefficients is assumed to be the preliminary CoG, that is X_{cog}=0.5153L_{ref}; Y_{cog}=0; Z_{cog}=−0.0124 L_{ref} .

Fig. 6 and Fig. 7 show that all the configurations are statically stable in longitudinal flight (e.g., Cm_{alpha}<0) for AoA higher than 2-3 deg, with the exception of the FTB-4_421 configuration.

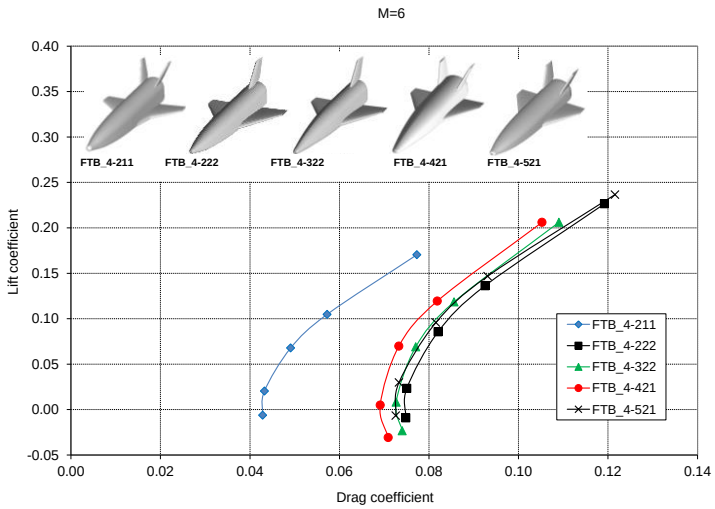

Fig. 4 FTB aerodynamic polars at M_∞=6

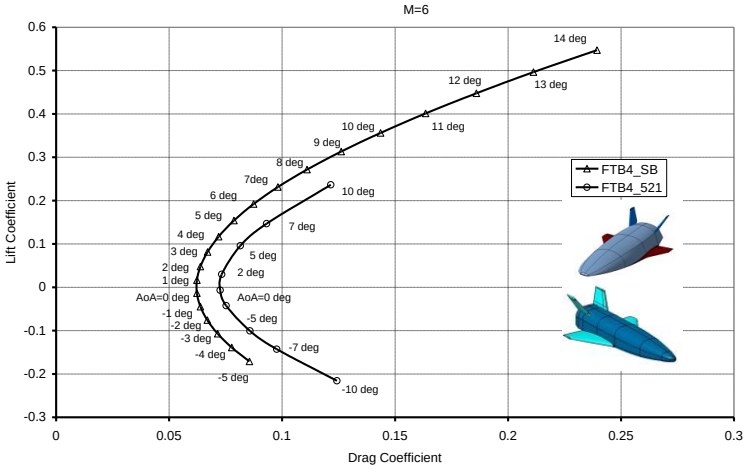

Fig. 5 FTB aerodynamic polars at M_∞=6 for winged and spatuled configurations

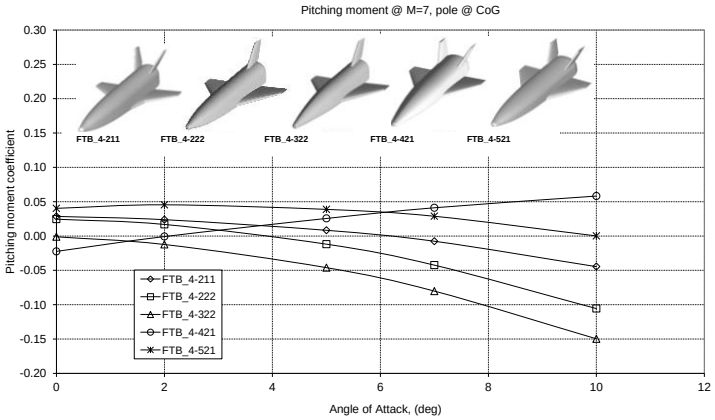

Fig. 6 Pitching moment coefficients at M_∞=7

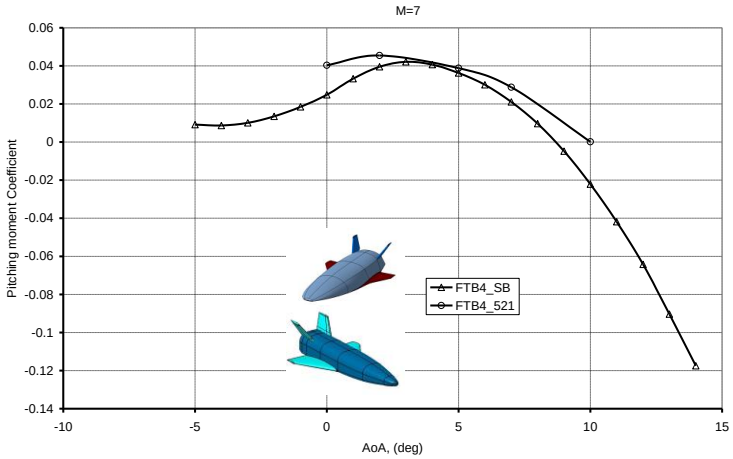

Fig. 7 Pitching moment coefficients at M_∞=7

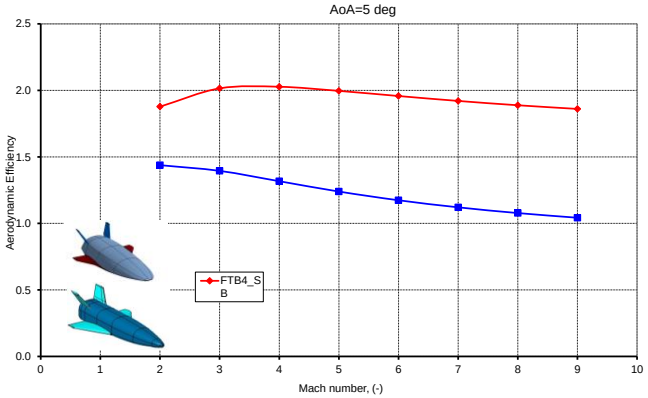

Fig. 8 Lift-to-Drag ratio versus Mach at α=5 deg

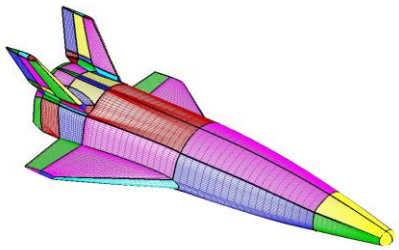

Fig. 9 Example of CFD surface mesh for the winged configuration

Anyway, design results highlight that the latter configuration can be trimmed (i.e., Cm=0) for AoA higher than 15 deg. In particular, the concepts SB and 521 are naturally trimmed respectively at about 8.5 and 10 deg in clean configuration. Finally, both configurations can be trimmed with flap positive deflection (i.e., downward) for positive AoA.

The lift-to-drag ratio of FTB 4-521 and SB is reported in Fig. 8 for Mach number ranging from 2 to 9 at α=5 deg, showing an average gain of 50% in aerodynamic efficiency with the SB configuration, as expected.

Then, FTB_4-SB is able to perform a reentry flight at a rather low AoA, thus flying like an airplane and not at a high AoA, as the classical reentry flight of the US Space Shuttle (Anderson 1989). As shown, the SB configuration shows an enhanced aerodynamic efficiency due to its higher aerodynamic lift together with a lower aerodynamic drag. Note that L/D is one of the most important features of the vehicle's aerodynamic performance. In fact, it has a direct impact on cross-range capability of the reentry vehicle that has to reach its nominal landing site at the end of space mission by unpowered flight.

As far as CFD analysis is concerned, on the base of the trajectory scenario a number of flight conditions have been selected, and a multiblock computational domain close to that recognized in Fig. 9 for the FTB-4_421 vehicle alone has been considered.

For example, Fig. 10 shows the static temperature field for the FTB-4_421 configuration when it is flying at M_∞=8 and α=10 deg. Streamtraces are also reported to highlight the flowfield past the vehicle. As shown, due to the slender concept configuration a narrow shock layer is expected to envelope the vehicle.

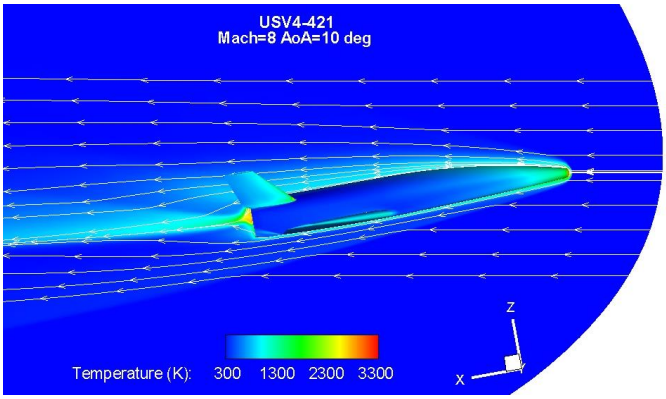

Fig. 10 Temperature contours at M_∞=8 and α=10 deg

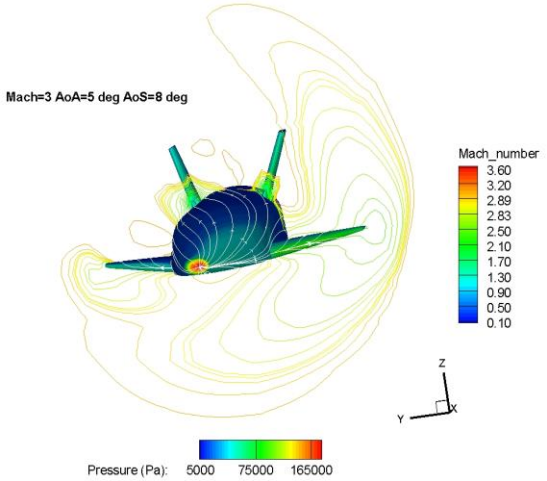

Fig. 11 Pressure contours at M_∞=8 and α=10 deg

The effect of sideslip angle on the flowfield past the winged body configuration can be appreciated in Fig. 11 for M_∞=3, α=5 deg and β=8 deg.

In particular, the figure displays the pressure contours on vehicle surface and Mach number contours on a cross plane cutting the wing. The asymmetric distribution of both the fluid dynamics features due to the angle of sideslip is clearly shown.

4. Aerothermodynamic analysis

Once the flight scenario of FTB_4 is provided, it dictates the aeroheating environment that the vehicle concept has to withstand along its lifting reentry flight. During flight, in fact, the FTB_4 suddenly heats due to the dissipation, in the boundary layer, of its high internal energy (potential and kinetic) by friction with the atmosphere. Indeed, by flying the work did by aerodynamic drag in braking the vehicle heats the surface with a severity that depends on the reentry vehicle configuration (Anderson 1989). Therefore, stagnation points on the vehicle fuselage and on

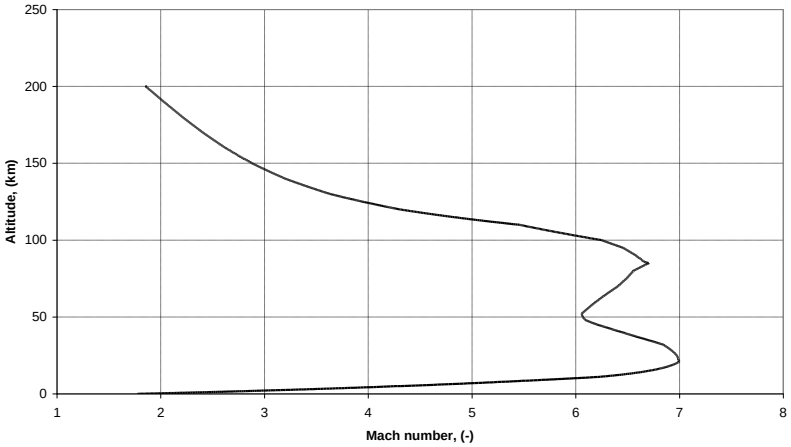

Fig. 12 Sub-orbital re-entry trajectory in the altitude-Mach map

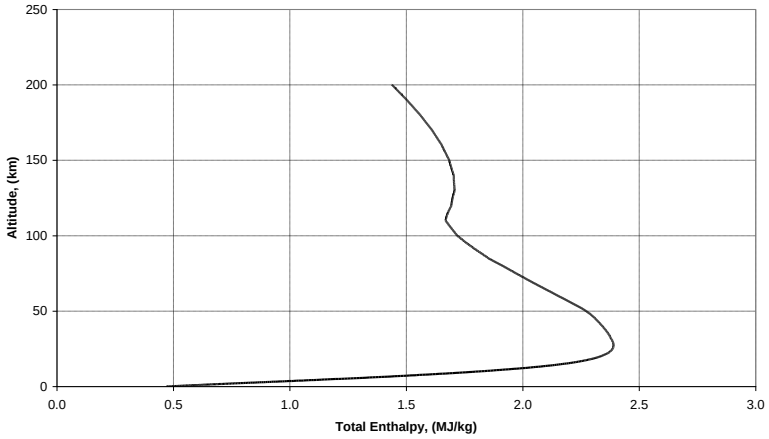

Fig. 13 Sub-orbital re-entry trajectory in the altitude-Total Enthalpy map

different wing sections have been monitored as reference control points to characterize the FTB_4 aerothermal environment.

4.1 Preliminary evaluation of nose and wing leading edges aeroheating

Aim of this section is to provide a preliminary overview of the aerothermal environment foreseen for both the spatuled and winged configurations of the FTB_4 vehicle concept.

The trajectory considered for the analysis is described in both Fig. 12 and Fig. 13 where the main trajectory parameters are reported. As shown, the peak of the total enthalpy (H_o) versus altitude for the considered trajectory is about 2.4 MJ/Kg at 25 Km of altitude. This very low energetic value allows neglecting any real gas effect.

In Fig. 14 and Fig. 15 the time histories of the stagnation point heat flux, both for cold and radiative cooled wall conditions, are reported for the winged and spatuled configurations, respectively. The wall temperature is assumed to be 300 K (i.e., cold wall boundary condition) and

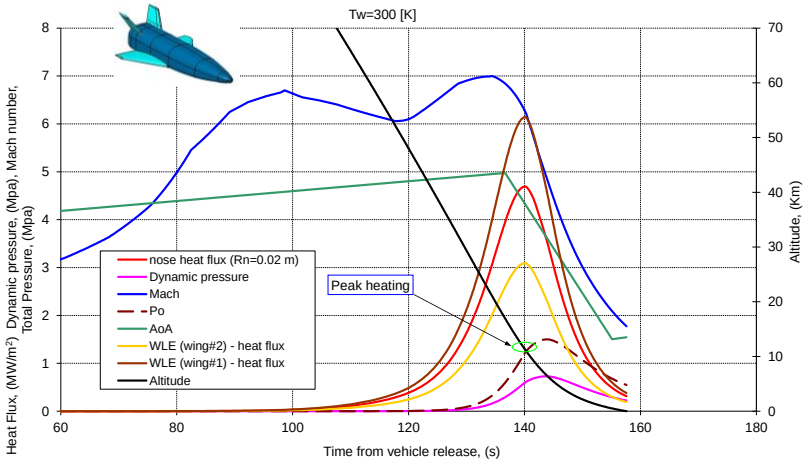

Fig. 14 Sub-orbital re-entry trajectory features for the WB (FTB-4_521) configuration

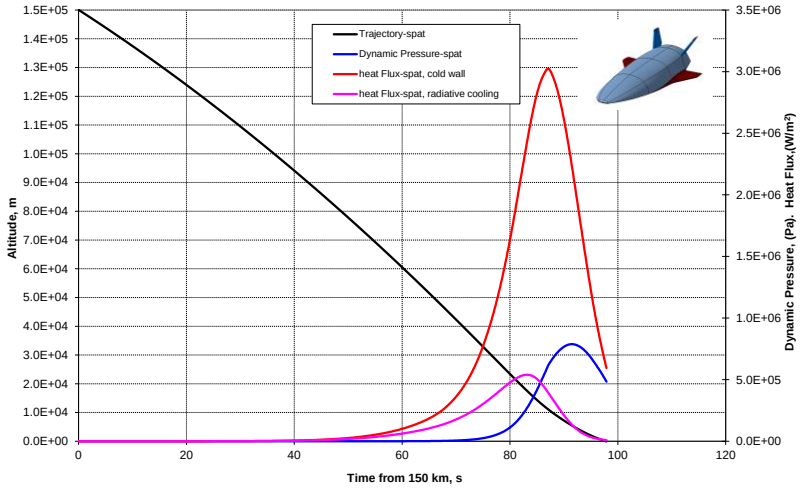

Fig. 15 Sub-orbital re-entry trajectory features for the SB configuration

the heat conduction inside the vehicle wall is neglected (i.e., $\dot{q}_{cond} = 0$). As shown, the nose peak heating is equal to about 5 and 3 MW/m^2 for WB and SB configuration, respectively. This high value is due to the high value of stagnation pressure occurring along the trajectory that compensates the small total enthalpy value.

In fact, the trajectory profile of stagnation point pressure, reported in Fig. 16, reaches about 1.4 MPa at a very low altitude (about 7 km).

However, due to the low values of H_0 the effect of wall temperature on heat flux shall be strong. Indeed, if we consider a radiative equilibrium assumption at the wall (i.e., $\dot{q}_{rad} = \sigma \varepsilon T_w^4$) the heat flux dramatically drops, as shown in Fig. 15 for the spatuled body configuration. Indeed, the heat flux at the stagnation point of SB configuration, for radiation cooled wall, decreases from 3 MW/m^2 to about 0.55 MW/m^2. Further, Fig. 15 also shows that the peak heating arises at a

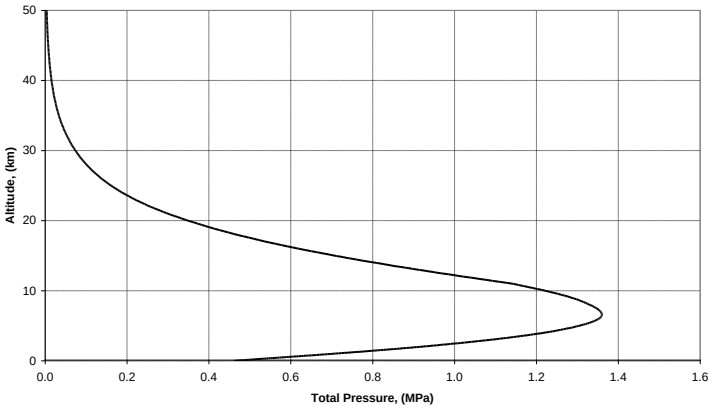

Fig. 16 Stagnation point pressure during descent

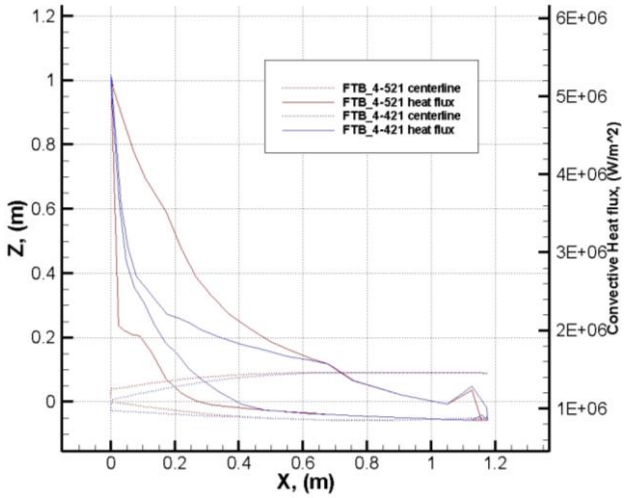

Fig. 17 Centerline heat flux (W/m^2) comparison between FTB4-421 and FTB4-521

higher altitude (H=17.6 Km) when the Mach number is equal to about 6.9.

Moreover, these values of heat flux are quite conservative since the peak heating occurs for a very limited time interval during the ending phase of the trajectory; so to obtain more realistic values also the heat transfer inside the nose (e.g., conductive heat flux) should be taken into account. For instance, at steady state conditions the energy balance, per unit time, at vehicle wall reads

$$\dot{q}_c - \dot{q}_{cond} - \dot{q}_{rad} = 0 \tag{1}$$

Anyway, FTB_4 reaches the trajectory peak heating at about M_∞=6.3 and 11.3 km altitude (cold wall). At these freestream (conservative) conditions a number of engineering-based analyses (e.g., 1-D boundary layer methods) have been performed in the case of turbulent flow conditions as a conservative estimation.

Some preliminary results can be recognized in Fig. 17 and Fig. 18 where the heat flux distribution along both the WB and SB centerlines is shown, respectively.

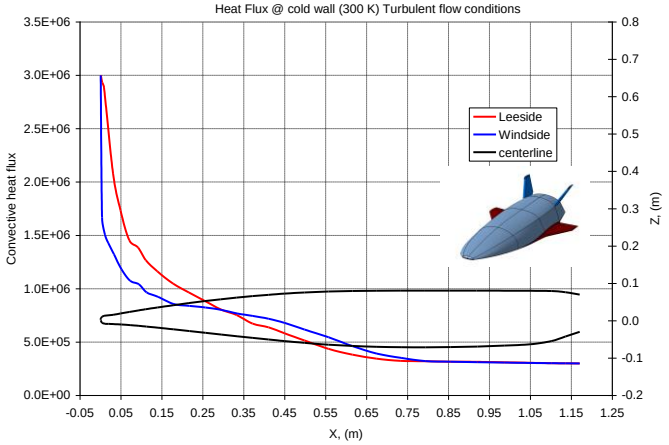

Fig. 18 Centerline heat flux (W/m^2) comparison for FTB4-SB

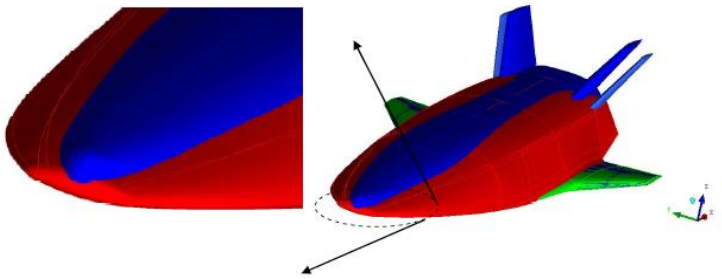

Fig. 19 Forebody comparison between FTB-4_421 (blue) and FTB-4_SB (red)

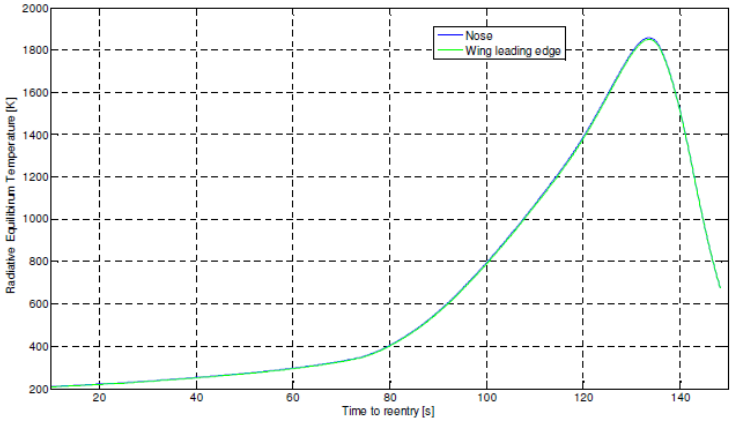

Fig. 20 Time history of nose and wing leading edges radiative equilibrium temperature (ε=0.8)

It is worth noting that the large differences in stagnation point heat flux (Fig. 17 and Fig. 18) can be explained by the comparison between the forebody of winged and spatuled configurations, as recognized in Fig. 19.

The time histories of radiative equilibrium temperature for both the nose and wing leading edges of SB configuration can be seen in Fig. 20. They appear quite the same due to a combined effect of both higher sweep angle and leading edges radius (wing #2).

In addition, the normalized heat flux distribution for the wing section at y=0.2 m of the SB configuration is reported in Fig. 21 for fully turbulent flow conditions.

Anyway, a conservative assessment of the wing leading edge aeroheating also requires taking into account the shock-shock interaction phenomenon (SSI), due to the interaction between the vehicle bow shock and the wing shock. This interaction causes an overshoot of both pressure and heat flux localized at the wing leading edge.

In particular the point of wing leading edge where this interaction impinges depends on the freestream conditions. For example, the SSI that takes place on the FTB_4-421 at M_∞=6, M_∞=7

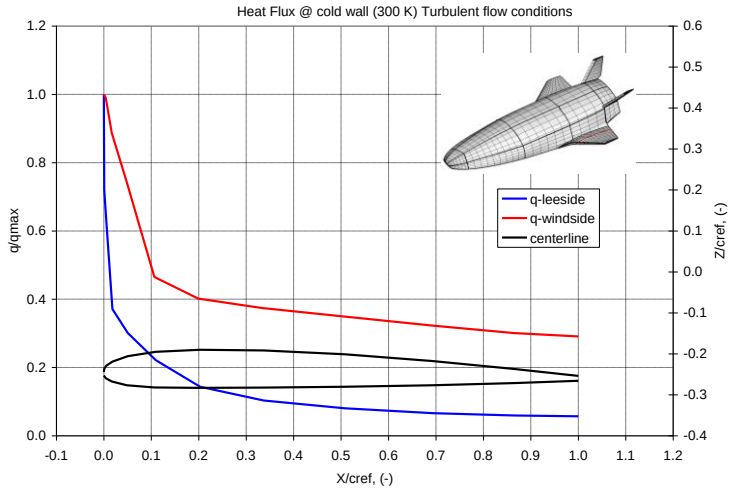

Fig. 21 Normalized heat flux distribution on the FTB_4-SB airfoil at y=0.2 m

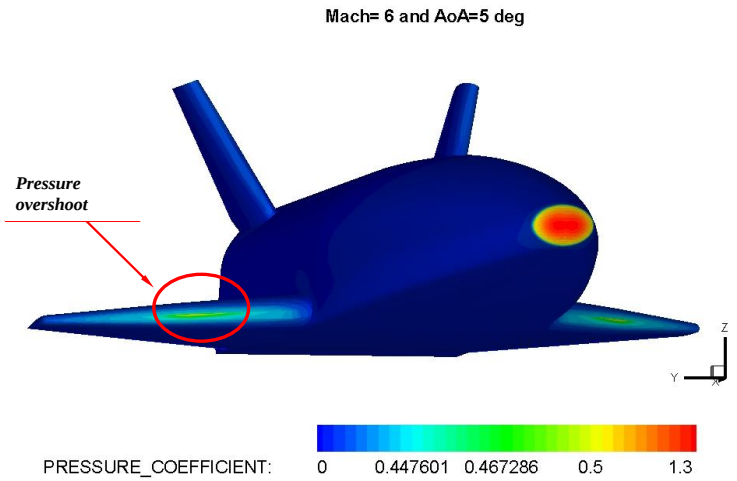

Fig. 22 Pressure coefficient distribution on FTB4-421 surface at M_∞=6 and α=5 deg

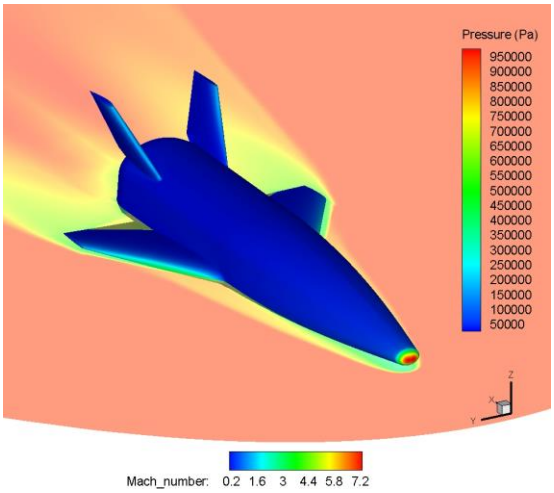

Fig. 23 Pressure and Mach number distributions on FTB4-421 surface and wing plane at M_∞=7 and α=5 deg

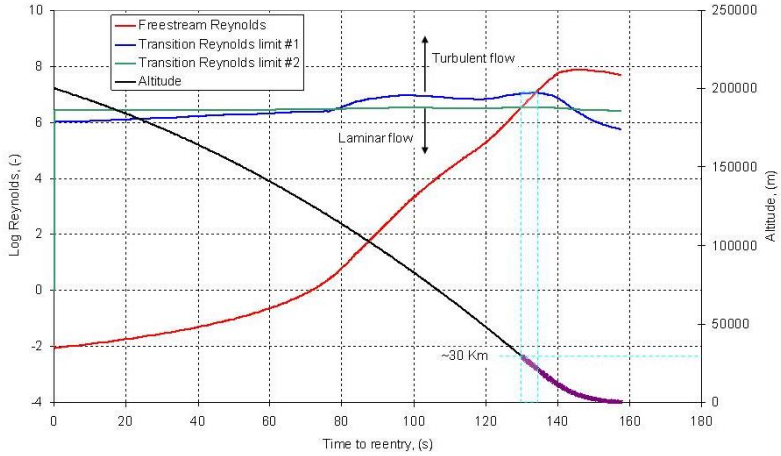

Fig. 24 Assessment of laminar-to-turbulent transition

and α=5 deg can be appreciated in Fig. 22 and Fig. 23, respectively.

Fig. 22 shows the contour plot of pressure coefficient on vehicle surface whereas Fig. 23 displays also the Mach number on the wing plane.

It is clearly shown the pressure overshoot where SSI impinges on the wing leading edge as well as the trace of bow shock on the wing plane (see Fig. 23). Therefore, for a reliable wing aeroheating estimation Navier-Stokes computations are mandatory as concept design matures.

Finally, a preliminary assessment of the laminar-to-turbulent transition has been also performed by means of the following two transition criteria

$$\begin{aligned} \mathrm{Log\,Re}_\infty &> \left[\mathrm{Log\,Re}_T + \mathrm{Cm}(\mathrm{M}_\infty)\right] \\ \mathrm{Log\,Re}_T &> 6.421\exp\left(1.209\,\mathrm{x}10^{-4}\,\mathrm{M}_e^{2.641}\right) \end{aligned} \tag{2}$$

where R_{eT} and Cm in the first relationship depend on the type of flow, AoA, leading edge sweep

angle, and leading edge nose bluntness (Quinn and Going 1990). They highlight that below 30 Km altitude turbulent flow conditions are expected, as clearly recognized in Fig. 24.

5. Conclusions

A summary review of the aerodynamic characteristic of a small hypersonic flying test bed, embodying the critical technologies and the features of an operational system, is provided. Such aerodynamic and aerothermodynamic characteristics, aimed to carry out preliminary databases compliant with a phase-A design level, are addressed by means of both 3-D supersonic-hypersonic panel method and Computational Fluid Dynamics analyses. The configuration chosen for the flying test bed is the result of a trade-off analysis involving several vehicle configurations. The winning configuration is the one showing, at the same time, the best aerodynamic and aerothermodynamic performance. Design analyses shown that for low angle of attack, say about 5 deg, the nose-up configurations are the best lifted ones and are statically stable in longitudinal flight for angle of attack higher than 2 deg. In particular, the FTB_4-521 configuration features a natural trim point at about α=10 deg. Therefore, it can be trimmed by positive flap deflections. Moreover, when the vehicle is flying at α=5 deg and M_∞=6 and 7 a flap deflection of about 7 and 10 deg allows to pitch trim the flying test bed, respectively. Finally, design analysis also points out that the spatuled body configuration features the best performance from both the aerodynamic efficiency and the aeroheating points of view. Indeed, the heat flux distributions, provided for radiative cooling condition at wall and thermal shield emissivity equal to 0.8, highlight that the vehicle heatshield has to withstand to about 600 kW/m^2 at nose leading edge which refer to the trajectory peak heating that the vehicle experiences at about M_∞=6.9 at 18.3 km altitude.

References

Anderson, J.D. (1989), *Hypersonic and High Temperature Gas Dynamics*, McGraw-Hill Book Company, New York.

Brauckmann, G.J. (1999), "X-34 vehicle aerodynamic characteristics", *J. Spacecraf. Rock*., **36(**2), 229-239.

De Matteis, P.P. and Russo, G. (2006), "The USV_X concept: mastering key-elements for future reentry systems", *Proceedings of 1st International ARA Days-Atmospheric Reentry Systems, Missions and Vehicles*, Arcachon, France.

Guidotti, G., Pezzella, G., Richiello, C., Russo, G., Tirtey, S.C. and Boyce, R.R. (2011), "Preliminary analysis of the USV_2 hypersonic flight test", *Proceedings of 7th European Symposium on Aerothermodynamics*, Brugge, Belgium.

Maughmer, M., Ozoroski, L., Straussfogel, D. and Long, L. (1993), "Validation of engineering methods for predicting hypersonic vehicle control forces and moments", *J. Guid. Control Dyn*., **16** (4), 762-769.

Moore, M.E. and Williams, J.E. (1989), "Aerodynamic prediction rationale for analyses of hypersonic configurations", *Proceedings of 27th Aerospace Sciences Meeting*, AIAA 89-0525.

Pezzella, G. (2011), "Aerodynamic and aerothermodynamic trade-off analysis of a small hypersonic flying test bed", *Acta Astronautica*, **69**(3), 209-222.

Pezzella, G., Gardi, R., Guidotti, G. and Richiello, C. (2011), "Aerodynamic and aerothermodynamic trade-off analysis of the italian USV2 flying test bed in the framework of an hypersonic flight test", *Proceedings of 3rd International ARA Days*, Arcachon, France, May.

Pezzella, G., Marini, M., Roncioni, P., Kauffmann, J. and Tomatis, C. (2009), "Preliminary design of vertical takeoff hopper concept of future launchers preparatory program", *J. Spacecraf. Rock.*, **46**(4), 788-799.

Prabhu, D.K. (2004), "System design constraints-trajectory aerothermal environments", *RTO AVT/VKI Lecture Series in Critical Technologies for Hypersonic Vehicle Development*, May.
Quinn, R.D. and Gong, L. (1990), "Real-time aerodynamic heating and surface temperature calculations for hypersonic flight simulation", *NASA Technical Memorandum*, 4222.
Russo, G. (2011), "USV status 2011: new steps ahead", *Proceedings of 17th AIAA International Space Planes and Hypersonic Systems and Technologies Conference*, San Francisco, April.
Russo, G. (2011), "USV programme progress and perspectives", *Proceedings of 3rd International ARA Days*, Arcachon, France, May.
Roncioni, P., Rufolo, G.C., Marini, M. and Borrelli, S. (2009), "CFD rebuilding of USV-DTFT1 vehicle in-flight experiment", *Acta Astronautica*, **66**(7), 1201-1219.
Viviani, A. and Pezzella, G. (2010), "Computational flowfield analysis over a Blunt-Body reentry vehicle", *J. Spacecraf. Rock.*, **47**(2), 258-270.

CC